Three-dimensional THz lumped-circuit resonators

Yanko Todorov, Pascal Desfonds, Cherif Belacel, Loic Becerra, Carlo Sirtori

Three-dimensional THz lumped-circuit resonators

Yanko Todorov,[1,*] Pascal Desfonds,[1] Cherif Belacel,[1] Loïc Becerra,[2] and Carlo Sirtori[1]

[1]*Laboratoire Matériaux et Phénomènes Quantiques, Université Paris Diderot, Sorbonne Paris Cité, CNRS-UMR 7162, 75013 Paris, France*

[2]*Institut des Nanosciences de Paris, Université Pierre et Marie Curie, UMR7588, 4 place Jussieu, 75252 Paris, France*

[*]*yanko.todorov@univ-paris-diderot.fr*

Abstract: Our work describes a novel three dimensional meta-material resonator design for optoelectronic applications in the THz spectral range. In our resonant circuits, the capacitors are formed by double-metal regions cladding a dielectric core. Unlike conventional planar metamaterials, the electric field is perpendicular to the surface and totally confined in the dielectric core. Furthermore, the magnetic field, confined in the inductive part, is parallel to the electric field, ruling out coupling through propagation effects. Our geometry thus combines the benefit of double-metal structures that provide parallel plate capacitors, while maintaining the ability of meta-material resonators to adjust independently the capacitive and inductive parts. Furthermore, in our geometry, a constant bias can be applied across the dielectric, making these resonators very suitable for applications such as ultra-low dark current THz quantum detectors and amplifiers based on quantum cascade gain medium.

OCIS codes: (160.3918) Metamaterials; (230.5750) Resonators; (260.3090) Infrared, far; (310.4165) Multilayer design.

References and links

1. W. Cai and V. M. Shalaev, *Optical Metamaterials: Fundamentals and Applications* (Springer, 2009).
2. M. A. Seo, H. R. Park, S. M. Koo, D. J. Park, J. H. Kang, O. K. Suwal, S. S. Choi, P. C. M. Planken, G. S. Park, N. K. Park, Q. H. Park, and D. S. Kim, "Terahertz field enhancement by a metallic nano-slit operating beyond the skin-depth limit," Nat. Photonics **3**(3), 152–156 (2009).
3. A. Benz, S. Campione, J. F. Klem, M. B. Sinclair, and I. Brener, "Control of strong light-matter coupling using the capacitance of metamaterial nanocavities," Nano Lett. **15**(3), 1959–1966 (2015).
4. M. W. Klein, C. Enkrich, M. Wegener, C. M. Soukoulis, and S. Linden, "Single-slit split-ring resonators at optical frequencies: limits of size scaling," Opt. Lett. **31**(9), 1259–1261 (2006).
5. S. A. Maier, "Plasmonic field enhancement and SERS in the effective mode volume picture," Opt. Express **14**(5), 1957–1964 (2006).
6. H. Tao, E. A. Kadlec, A. C. Strikwerda, K. Fan, W. J. Padilla, R. D. Averitt, E. A. Shaner, and X. Zhang, "Microwave and terahertz wave sensing with metamaterials," Opt. Express **19**(22), 21620–21626 (2011).
7. R. Singh, W. Cao, I. Al-Naib, L. Cong, W. Withayachumnankul, and W. Zhang, "Ultrasensitive terahertz sensing with high-*Q* Fano resonances in metasurfaces," Appl. Phys. Lett. **105**(17), 171101 (2014).
8. S. Collin, "Nanostructure arrays in free-space: optical properties and applications," Rep. Prog. Phys. **77**(12), 126402 (2014).
9. Y. N. Chen, Y. Todorov, B. Askenazi, A. Vasanelli, G. Biasiol, R. Colombelli, and C. Sirtori, "Antenna-coupled microcavities for enhanced infrared photo-detection," Appl. Phys. Lett. **104**(3), 031113 (2014).
10. A. Bonakdar and H. Mohseni, "Impact of optical antennas on active optoelectronic devices," Nanoscale **6**(19), 10961–10974 (2014).
11. H.-T. Chen, W. J. Padilla, M. J. Cich, A. K. Azad, R. D. Averitt, and A. J. Taylor, "A metamaterial solid-state terahertz phase modulator," Nat. Photonics **3**(3), 148–151 (2009).
12. G. Scalari, C. Maissen, D. Turcinková, D. Hagenmüller, S. De Liberato, C. Ciuti, C. Reichl, D. Schuh, W. Wegscheider, M. Beck, and J. Faist, "Ultrastrong coupling of the cyclotron transition of a 2D electron gas to a THz metamaterial," Science **335**(6074), 1323–1326 (2012).
13. Y. Todorov and C. Sirtori, "Few-electron ultrastrong light-matter coupling in a quantum LC circuit," Phys. Rev. X **4**, 041031 (2014).

#237703 Received 8 Apr 2015; revised 12 May 2015; accepted 12 May 2015; published 17 Jun 2015

Corrected: 19 October 2015

14. Y. C. Jun, J. Reno, T. Ribaudo, E. Shaner, J.-J. Greffet, S. Vassant, F. Marquier, M. Sinclair, and I. Brener, "Epsilon-near-zero strong coupling in metamaterial-semiconductor hybrid structures," Nano Lett. **13**(11), 5391–5396 (2013).
15. A. Benz, S. Campione, S. Liu, I. Montaño, J. F. Klem, A. Allerman, J. R. Wendt, M. B. Sinclair, F. Capolino, and I. Brener, "Strong coupling in the sub-wavelength limit using metamaterial nanocavities," Nat. Commun. **4**, 2882 (2013).
16. D. Dietze, A. Benz, G. Strasser, K. Unterrainer, and J. Darmo, "Terahertz meta-atoms coupled to a quantum well intersubband transition," Opt. Express **19**(14), 13700–13706 (2011).
17. S. Campione, A. Benz, J. F. Klem, M. B. Sinclair, I. Brener, and F. Capolino, "Electrodynamic modeling of strong coupling between a metasurface and intersubband transitions in quantum wells," Phys. Rev. B **89**(16), 165133 (2014).
18. C. Walther, G. Scalari, M. I. Amanti, M. Beck, and J. Faist, "Microcavity laser oscillating in a circuit-based resonator," Science **327**(5972), 1495–1497 (2010).
19. B. Paulillo, J. M. Manceau, A. Degiron, N. Zerounian, G. Beaudoin, I. Sagnes, and R. Colombelli, "Circuit-tunable sub-wavelength THz resonators: hybridizing optical cavities and loop antennas," Opt. Express **22**(18), 21302–21312 (2014).
20. J. D. Jackson, *Classical Electrodynamics*, (John Wiley & Sons, 1999).
21. I. Bahl, *Lumped Elements for RF and Microwave Circuits* (Artech House, 2003).
22. J.-J. Greffet, M. Laroche, and F. Marquier, "Impedance of a nanoantenna and a single quantum emitter," Phys. Rev. Lett. **105**(11), 117701 (2010).
23. M. S. Vitiello, D. Coquillat, L. Viti, D. Ercolani, F. Teppe, A. Pitanti, F. Beltram, L. Sorba, W. Knap, and A. Tredicucci, "Room-temperature terahertz detectors based on semiconductor nanowire field-effect transistors," Nano Lett. **12**(1), 96–101 (2012).
24. R. P. Feynman, R. B. Leighton, and M. Sands, *The Feynman Lectures on Physics: Mainly Electromagnetism and Matter, Vol. 2* (Addison-Wesley, 1977).
25. H. A. Haus and J. R. Melcher, *Electromagnetic Fields and Energy*. (Massachusetts Institute of Technology: MIT OpenCourseWare). http://ocw.mit.edu (accessed March 6, 2015). License: Creative Commons Attribution-NonCommercial-Share Alike.
26. J. Madéo, Y. Todorov, and C. Sirtori, "Antenna-coupled microcavities for terahertz emission," Appl. Phys. Lett. **104**(3), 031108 (2014).
27. E. Strupiechonski, G. Xu, M. Brekenfeld, Y. Todorov, N. Isac, A. M. Andrews, P. Klang, C. Sirtori, G. Strasser, A. Degiron, and R. Colombelli, "Sub-diffraction-limit semiconductor resonators operating on the fundamental magnetic resonance," Appl. Phys. Lett. **100**(13), 131113 (2012).
28. E. Strupiechonski, G. Xu, P. Cavalié, N. Isac, S. Dhillon, J. Tignon, G. Beaudoin, I. Sagnes, A. Degiron, and R. Colombelli, "Hybrid electronic-photonic sub-wavelength cavities operating at THz frequencies," Phys. Rev. B **87**(4), 041408 (2013).
29. Y. Todorov, L. Tosetto, J. Teissier, A. M. Andrews, P. Klang, R. Colombelli, I. Sagnes, G. Strasser, and C. Sirtori, "Optical properties of metal-dielectric-metal microcavities in the THz frequency range," Opt. Express **18**(13), 13886–13907 (2010).
30. C. Feuillet-Palma, Y. Todorov, R. Steed, A. Vasanelli, G. Biasiol, L. Sorba, and C. Sirtori, "Extremely sub-wavelength THz metal-dielectric wire microcavities," Opt. Express **20**(27), 29121–29130 (2012).
31. C. Hoer and C. Love, "Exact inductance equations for rectangular conductors with application to more complicated geometries," J. Res. NBS **69C**, 127 (1965).
32. N. Laman and D. Grischowsky, "Terahertz conductivity of thin metal films," Appl. Phys. Lett. **93**(5), 051105 (2008).
33. H. B. Palmer, "Capacitance of a parallel-plate capacitor by the Schwartz-Christoffel transformation," Trans. AIEE **56**, 363 (1927).
34. Y. Y. Iossel, E. S. Kochanov, and M. G. Strunskiy, *Raschet elektricheskoy yemkosti* (*Calculation of Electric Capacitance*) (Energoizdat, 1981).
35. M. Geiser, F. Castellano, G. Scalari, M. Beck, L. Nevou, and J. Faist, "Ultrastrong coupling regime and plasmon polaritons in parabolic semiconductor quantum wells," Phys. Rev. Lett. **108**(10), 106402 (2012).
36. M. Geiser, C. Walther, G. Scalari, M. Beck, M. Fischer, L. Nevou, and J. Faist, "Strong light-matter coupling at terahertz frequencies at room temperature in electronic LC resonators," Appl. Phys. Lett. **97**(19), 191107 (2010).

1. Introduction

Metamaterials rely on arrays of miniature circuit-resonators, such as split-rings, that can confine the electromagnetic field into sub-wavelength volumes [1], down to nanometer sizes [2–4]. This property allows highly efficient surface sensing [5–7], very low-dark current quantum detectors [8–10], modulators [11] and new schemes for exploring the ultra-strong light-matter interaction [3, 12–14]. The majority of meta-materials, regardless their operation frequency are obtained by using a two-dimensional planar technology [3, 14, 15]. The interaction between the electric field and the active material hosted in the substrate is therefore not optimized as it relies only on the fringing fields that leak out from the circuit capacitor [16, 17]. In the THz region, other designs for metamaterial-like *LC*-resonators based

#237703 Received 8 Apr 2015; revised 12 May 2015; accepted 12 May 2015; published 17 Jun 2015

on double-metal geometries have been proposed [18, 19], with the advantage to optimize the field confinement within the dielectric core. Our design introduces a substantial difference with the previously reported structures, where the electric and magnetic field are *orthogonal* when calculated in the same plane. In our configuration the dominant electric and magnetic field components (E_z and H_z) are *parallel* to each other in a plane crossing half a way the capacitor. This parallelism between the magnetic and electric field is essential to exclude propagation effects, since such configuration with parallel electric and magnetic fields cannot satisfy the Helhmoltz wave equation [20]. As a result, the inductive and the capacitive parts can be adjusted independently for a fixed THz frequency of operation, similarly to the case of lumped element electronic circuits [21]. Three-dimensional resonators based on this design have been demonstrated across the whole THz range (1-20 THz). This architecture allows for ultra-sub-wavelength electric field confinement in a dielectric core, opening new possibilities for advanced opto-electronic devices, such as emitters [18, 22] and detectors of infrared radiation, based on a single quantum object [23].

2. Resonator design, characterization and modelling

The resonator design investigated in this work is depicted in Fig. 1(a). It consists of a ground strip (rectangular metallic patch), deposited on substrate, a dielectric layer of thickness T (transparent in Fig. 1(a)) that covers the ground strip and a Π–shaped half ring deposited just above the strip. Figures 1(b) and 1(c) show realization of the structure in an array of resonators on a GaAs substrate, with the metallic parts made of gold (150nm thick) and T = 2μm thick dielectric SiO_2 layer. In Fig. 1(c) we also define the geometrical parameters W, L_x and L_y that have been varied in this work, while the width E of the Π–ring is kept fixed at 2μm. The key feature of this structure is that the geometrical overlaps between the upper ring and the ground plate are acting as the plates of two capacitors. The capacitors localize the electric field into the SiO_2 dielectric, within a strongly sub-wavelength volume. This feature is confirmed by finite difference simulations of the electric E_z [Fig. 1(e)] and magnetic H_z [Fig. 1(f)] fields. In the bottom part of Figs. 1(e) and 1(f) the total electric and magnetic energy densities are also shown. While the electric filed is confined mostly in the capacitive parts [Fig. 1(e)], the magnetic field is localized around the loop formed by the upper ring and the ground plate [Fig. 1(f)]. This spatial separation of the electric and magnetic energy is reminiscent of the quasi-static nature of our resonator, in which the energy exchange is driven by the real current in the metallic parts, rather than propagative coupling in the bulk of the resonator [20, 24, 25]. This is a crucial point, as it allows to adjust independently the capacitance C and the inductance L of the structure, while the resonant frequency $f_{res} = 1/2\pi(CL)^{1/2}$ is kept fixed. Furthermore, as seen from the simulations from Figs. 1(e) and 1(f) the electric and magnetic fields components in the plane of the capacitors ("*xy*-plane") are parallel to each other, ruling out any possible coupling mediated by propagation effects. The reduction of the capacitive part can then lead to highly subwavelength volumes V_{capa} for the electric energy density, possibly down to nanoscale range, with corresponding high electric field amplitudes, $E = (hf_{res}/\varepsilon\varepsilon_0 V_{capa})^{1/2}$.

#237703 Received 8 Apr 2015; revised 12 May 2015; accepted 12 May 2015; published 17 Jun 2015

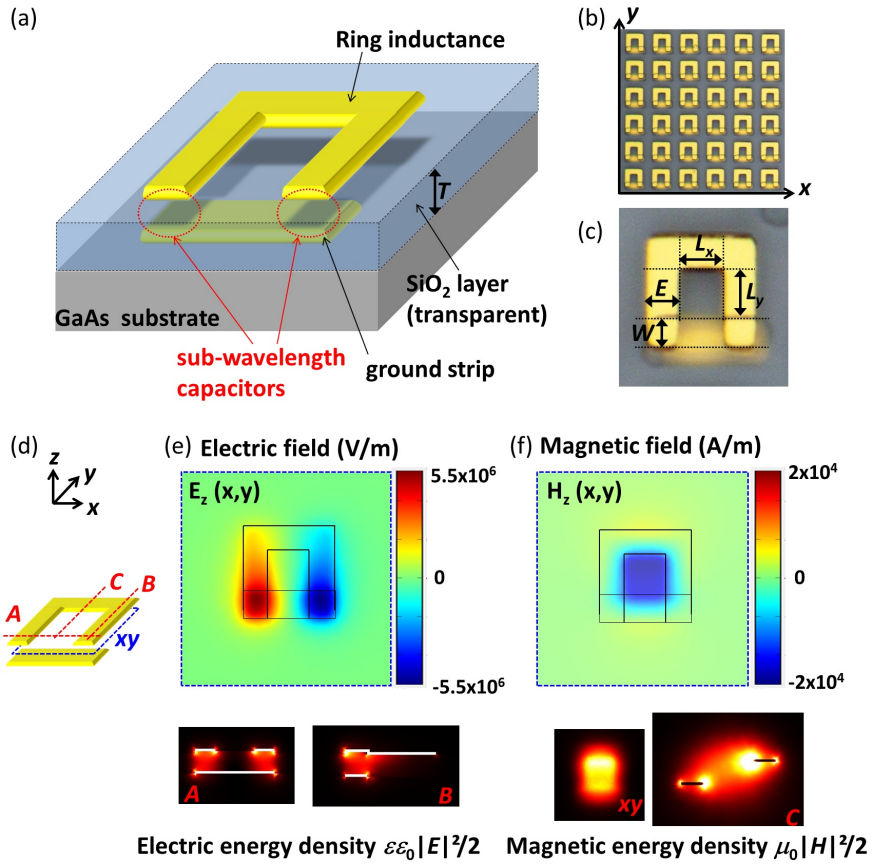

Fig. 1. (a) Perspective drawing of the resonator, indicating the subwavelength capacitor parts. (b,c) Microscope pictures of arrays realized by laser lithography on GaAs substrate and with SiO_2 dielectric layer. The main geometrical parameters are indicated in (c). (d) Coordinate system and a set of planes chosen for the illustration of the electromagnetic field distribution. The surfaces *A*, *B* and *C* are contained by the dashed lines and the *z*-direction. (e) Upper panel: electric field component E_z in the (*x*,*y*)-plane from (d). Lower panel: electric energy density plotted in the planes *A* and *B*. (f) Upper panel: magnetic field component H_z in the (*x*,*y*)-plane. Lower panel: magnetic energy density in the planes (*x*,*y*) and *C*.

In order to demonstrate that the resonant frequency can be tuned separately through the capacitive and inductive parts, we prepared arrays of resonators where the dimensions of the parameters W, L_x and L_y were varied from 2μm to 8μm, keeping a dielectric thickness T = 2μm. This allowed us to vary independently the capacitor size W, and the perimeter of the inductive loop $L_x + L_y$. In Figs. 2(a), 2(b), 2(c) we report the reflectivity spectra for three different families of parameters: (W = 2μm, L_x , L_y = 2μm), (W = 2μm, L_x = 2μm, L_y) and (W = 4μm, L_x = L_y), for light incident at θ = 10° with respect to the normal of the array. In Fig. 2(d) we also report measurements for a dielectric thickness T = 1μm. Reflectivity spectra with θ = 45° and θ = 60° yield essentially the same results and are not shown. We also performed transmission measurements, however the resonances were in that case less pronounced than in the reflectivity spectra. The measurements were performed with light polarized perpendicular to the two capacitors (along the *x*-direction). The resonator modes of the structure are clearly seen as the reflectivity minima of the spectra. The shaded band corresponds to the phonon absorption band of the GaAs substrate. In Fig. 2(a) we observe sharp reflectivity dips, while in Figs. 2(b) and 2(c) we rather observe Fano-type features with a reflectivity maximum immediately following the less pronounced resonant dips. These features probably arise from the increased radiation loss of the structure due to the inductive

#237703 Received 8 Apr 2015; revised 12 May 2015; accepted 12 May 2015; published 17 Jun 2015

loop [19, 26]. It is remarkable that, apart from the quasi-static mode illustrated in Fig. 1, we do not observe any higher order modes (in the range 1-20 THz) that are typically present in other types of resonators [19, 27–30].

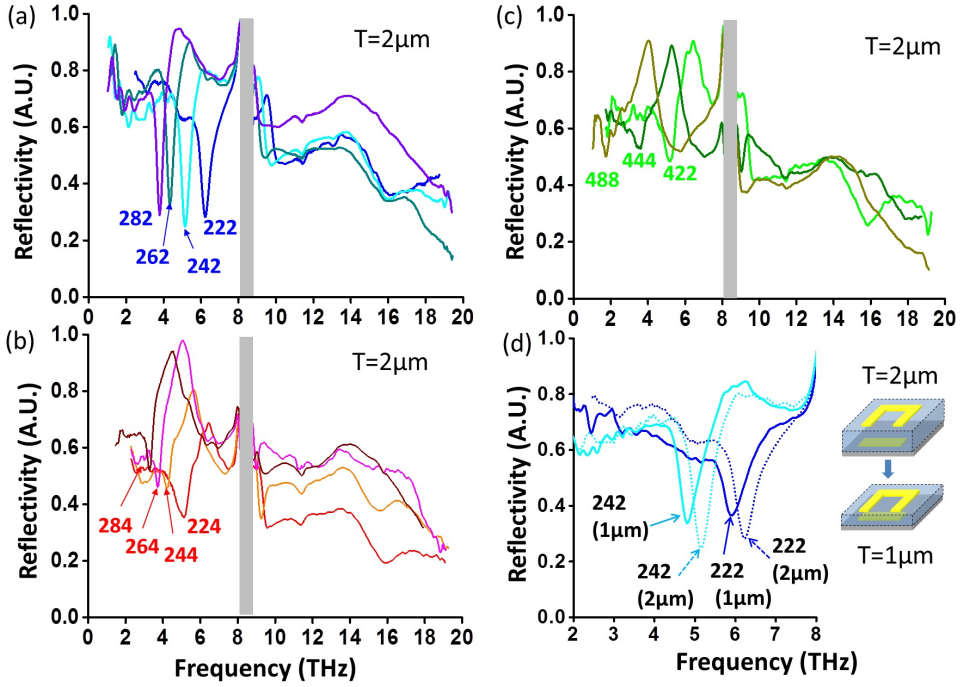

Fig. 2. (a,b,c) Experimental reflectivity spectra of resonator arrays such as the one depicted in Fig. 1(c), with light polarized along the two capacitors, and under almost normal incidence on the array surface. The thickness is $T = 2\mu m$. The triplet of numbers indicates the parameters (W L_x L_y) defined in Fig. 1(c), for instance 264 indicates nominal values $W = 2\mu m$, $L_x = 6\mu m$ and $L_y = 4\mu m$. (d) Spectra of the resonators 222 and 242 for two different thicknesses $T = 2\mu m$ (dotted curves) and $T = 1\mu m$ (continuous lines). The grey area corresponds to the phonon absorption of the GaAs substrate.

In Fig. 3, we plot the resonant frequencies extracted from the spectra in Fig. 2 as a function of a "scale parameter" p, defined as $p = (1/\sqrt{EW/T})(1/\sqrt{L_x + L_y})$ with $E = 2\mu m$ the thickness of the Π-ring. The definition of p is motivated by the formula of the resonant frequency $f_{res} = 1/2\pi(CL)^{1/2}$ as a function of the capacitance C and the inductance L of the structure. Indeed, we expect that the capacitance is roughly proportional to EW/T, while the inductance L is proportional to the perimeter $2(L_x + L_y)$. From Fig. 3 we observe that indeed f_{res} has an essentially linear dependence on p. Note that from this plot we used the parameters E, W, L_x, L_y measured for the real structures shown in the left panel of Fig. 3. From Fig. 3, we can note that the pairs of structures (242, 224), (244, 262) and (282, 264) that have similar loop perimeter $L_x + L_y$ also have identical frequencies, as expected. Furthermore, almost the same frequency is recovered by shrinking the loop and increasing the capacitor, as seen for the pair (444, 284) and the triplet (422, 224, 242). This indicates clearly that, provided the resonant frequency f_{res}, the inductive part and the capacitive part can be adjusted separately so that very sub-wavelength values of the electric field confinement volumes V_{capa} are achieved.

#237703 Received 8 Apr 2015; revised 12 May 2015; accepted 12 May 2015; published 17 Jun 2015

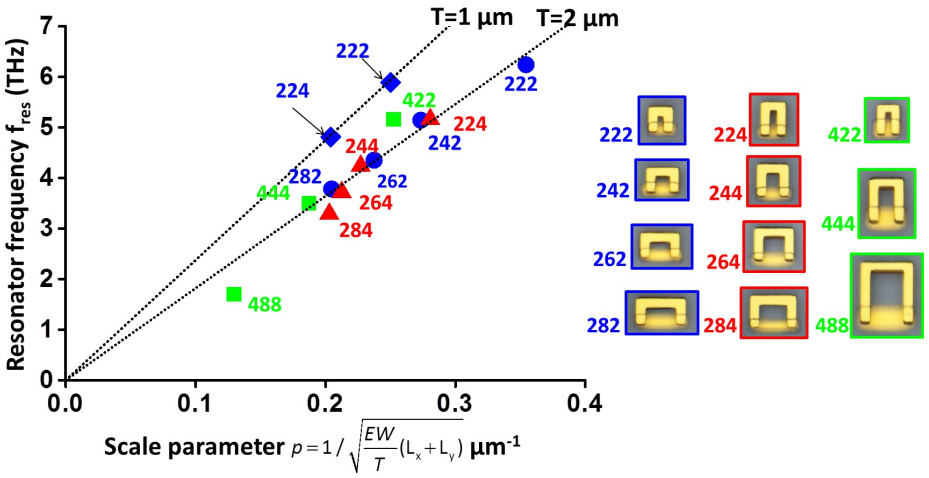

Fig. 3. Left: plot of the resonator frequencies measured from the data in Fig. 3 as a function of the "scale parameter" p, that is roughly proportional to the square root of the inverse of the product of the capacitance and inductance of the structure, as explained in the main text. Right: pictures of the different family of resonators.

In order to understand fully the dependence of the resonant frequency on the shape of the structures, we developed a lumped element model that is described in Fig. 4. Figure 4(a) presents the equivalent circuit with the correspondence to the geometrical parts that play role to inductances and capacitors. The total inductance is defined as $L = L_1 + L_2 + L_3 + L_4 - 2M_{13} - 2M_{24}$, where L_i are the self-inductances of the rectangular blocks indicated by numbers in Fig. 4(a) and the M_{ij} are the corresponding mutual inductances. The values of L_i and M_{ij} are computed with the exact formulas of Hoer and Love for thin tapes [31], as the skin dept of the metal is much smaller than the lateral size of the blocks at this frequency range [32]. The computed values of L are plotted in Fig. 4(b) as a function of the half-perimeter $L_x + L_y$. The total inductance is monotonic function of $L_x + L_y$ as anticipated, but more than linear because of the logarithmic factors in the exact expressions [31]. The mutual inductance accounts typically for 20% of the total inductance.

The full capacitance of the system consists of the double metal parts with capacitances C, highlighted in Fig. 4(a), and also of the mutual capacitance C_{inter} of the ring gap. To compute C_{inter}, we have used the formulas for slotline [20]. For the double-metal capacitors, we use the two dimensional version of the Palmer formula [33, 34]:

$$C = \varepsilon\varepsilon_0 \frac{WE}{T}\left\{1+\frac{T}{\pi E}\left(1+\ln\left[\frac{2\pi E}{T}\right]\right)\right\}\left\{1+\frac{T}{\pi W}\left(1+\ln\left[\frac{2\pi W}{T}\right]\right)\right\}. \qquad (1)$$

Besides the contribution of the double-metal region (factor WE/T), this formula contains corrections due to the fringing fields [33, 34]. Typical values for C from Eq. (1) are hundreds of aF, while for C_{inter} we obtain tens of aF, showing that indeed the majority of the electric energy of the resonator is located inside the dielectric core. The total capacitance $C/2 + C_{inter}$ is plotted in Fig. 4(c). Moreover, by decreasing the thicknesses T below 0.5µm C_{inter} becomes completely negligible. However, for capacitors with aspect ratio close to 1 the Palmer expression predict values that are considerably higher than the parallel plate formula $C = \varepsilon\varepsilon_0 WE/T$.

With the inductances and capacitances of the system determined, we have computed the resonant frequencies by solving the electrical circuit in Fig. 4(a). In Fig. 4(d) we compare the results with experiments (red squares). Very good match is observed for all structures, while the small discrepancies can be attributed to the uncertainty in the measured values of the

#237703 Received 8 Apr 2015; revised 12 May 2015; accepted 12 May 2015; published 17 Jun 2015

geometrical parameters. Furthermore, as seen in Fig. 4(d) the resonant frequencies are also well accounted by the simplified formula $f_{LC} = 1/2\pi[(C/2 + C_{inter})L]^{1/2}$ (blue open squares).

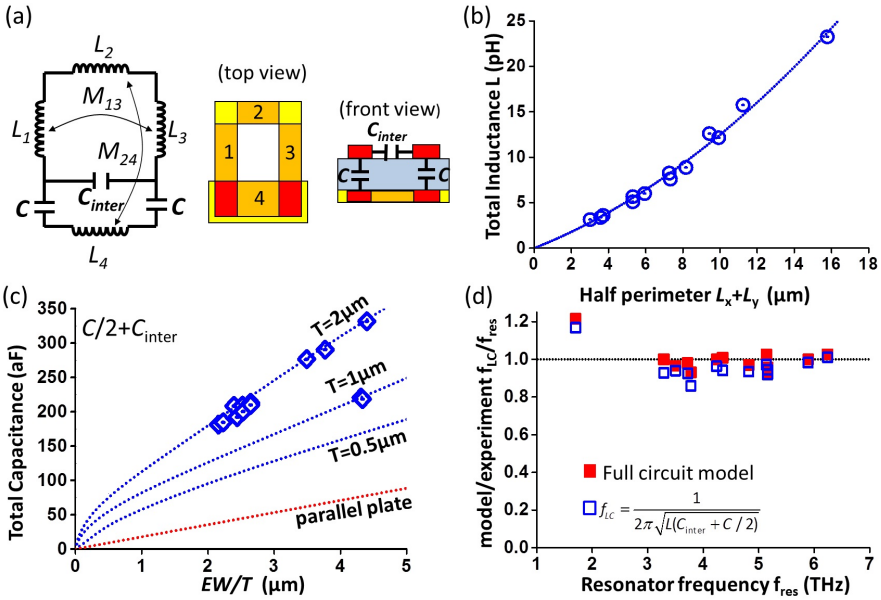

Fig. 4. Circuit model of the structure. (a) Scheme of the equivalent circuit, with indication of the inductive and capacitive elements. (b) Total inductance as a function of the half-perimeter $L_x + L_y$ of the magnetic loop (circles). The dotted line is a quadratic fit. (c) Total capacitance as a function of the parameter EW/T (diamonds). The dotted lines are extrapolation of the circuit model for decreasing capacitor surface EW, for a thickness T = 2μm, 1μm or 0.5μm of the dielectric layer. The red line is the parallel plate capacitor value $C/2 = 0.5\varepsilon\varepsilon_0 WE/T$. (d) Ratio f_{LC}/f_{res} between the modelled (f_{LC}) and measured frequencies (f_{res}) as a function f_{res}. The full squares are the values obtained with the full circuit model from Fig. 4(a), while the open squares are the values of the simplified formula $f_{LC} = 1/2\pi[(C/2 + C_{inter})L]^{1/2}$.

To ensure whether a resonator operates in the limit of propagation or in the quasi-static limit it is very convenient to use the well-known *size vs. wavelength* criterion, which sets that the quasi-static regime is the case where $\lambda << \lambda_{res}$ with λ a typical resonator size [20, 24, 25]. This limit is easily attained in all high frequency electronic devices up to tens of GHz, but has to be refined for the case of THz resonators that operate typically at the cross-over between optics and electronics [19, 28]. For this purpose, rather than the physical length λ, we use the maximum optical path L_{opt}, proportional to $n\lambda$, (n is the refractive index of the resonator) defined as the distance for a photon to propagate back and forth within the resonator. It is easy to understand that in the propagation regime a resonator sustains standing waves with resonant wavelengths λ_{res} such as $L_{opt} = K\lambda_{res}$ where K is an integer. The ratio L_{opt}/λ_{res} then quantifies the limit between propagation effects, where L_{opt}/λ_{res} = 1, 2, 3…, and the quasi-static regime, where $L_{opt}/\lambda_{res}<<1$. In Fig. 5 we have applied this criterion to the fundamental mode of several types of resonators: wires [30] ($L_{opt} = 2n\lambda$), the "*LC*" resonators from Ref [18, 35, 36], where $L_{opt} = 2n(2r + l)$ (r is the radius of the "capacitive" part and l the length of the "inductive" part), with n = 3.5 (GaAs dielectric core). We have also included the "monopolar" disk resonators from Refs [19, 27, 28]. where $L_{opt} = 4nD$ (D is the diameter of the disk resonators) for Ref [27], and $L_{opt} = 4(nD + d)$ for Ref [19], where the inductive part of length d is standing in the air. The factor 4 comes from the fact that this resonator can be interpreted as $\lambda_{res}/4$ standing wave with a maximum of the electric field in the capacitor and zero in the inductive loop. For the structures reported here, we use $L_{opt} = 2n((W + L_y)^2 + L_x^2)^{1/2}$ with n = 2 (SiO_2 dielectric core). As another criteria for our structure, we can take an optical path $L_{opt} = 2[2nW + L_x + L_y]$, which yields similar, but slightly higher values for L_{opt}/λ_{res} compared to those reported in Fig. 5. The results summarized in Fig. 5 show that the

#237703 Received 8 Apr 2015; revised 12 May 2015; accepted 12 May 2015; published 17 Jun 2015

structures from Ref [19]. indeed satisfy the quasi-static condition, in particular for very large wavelengths, $\lambda_{res} > 100\mu m$, whereas our resonator operates well within the quasi-static limit for the entire THz range.

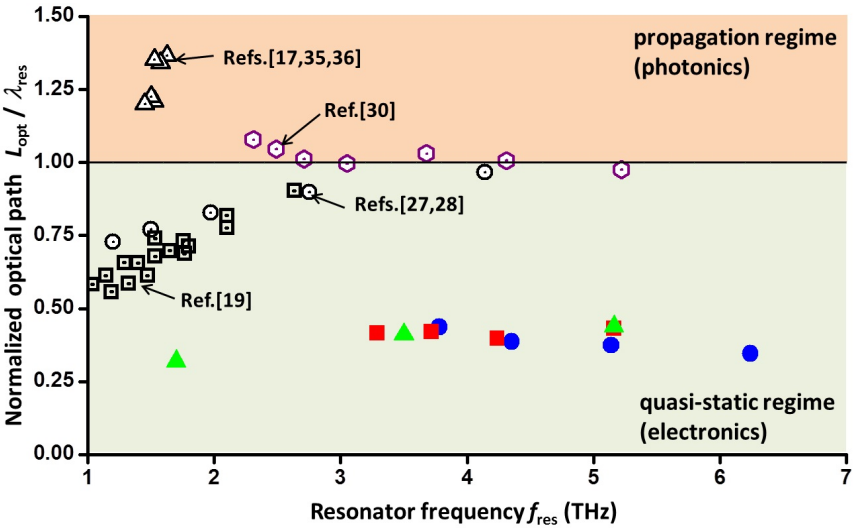

Fig. 5. Ratio between the minimal photon optical path L_{opt} and the resonant wavelength $\lambda_{res} = c/f_{res}$ for different resonators reported in the literature (open dotted symbols) as comparison to our work (full symbols, with the same code as in Fig. 3). The case $L_{opt}/\lambda_{res} = 1$ corresponds to the first standing wave mode in the structure. Higher order modes are provided by the condition $L_{opt}/\lambda_{res} = K$, where K is positive integer. The case $L_{opt}/\lambda_{res} < 1$ corresponds to resonators operating in the quasi-static regime. For simplicity, in this diagram we used the bulk refractive index of the dielectric filling the resonators; $L_{opt}/\lambda_{res} > 1$ signifies that the effective index of the guided mode is higher than the bulk refractive index.

3. Conclusion

In summary, we have reported three dimensional THz resonator architectures with a very sub-wavelength effective volume of the capacitive parts. An extrapolation of our circuit model shows that, by reducing the widths E and W and the thickness T volumes as small as $0.02\mu m^3$ can be achieved in the 1-10 THz range while the inductive loop is kept at sub-wavelength dimensions $L_x = L_y \sim 5\mu m$. In this limit the electric field is well localized within the capacitor and almost perfectly polarized in the z-direction. Such structures are therefore very suitable for studying the ultra-strong coupling regime with intersubband transitions, in the few electron limit [13]. Clearly, in such small volumes light harvesting could become problematic, as the impedance of our resonator $Z = (L/C)^{1/2}$ strongly mismatches the free space value 377 Ω. However this issue can be overcome by employing side antenna coupling [26]. Another advantage of our architectures is that they naturally allow applying a bias between the ground plate and the Π–ring, as required for optoelectronic applications.

Acknowledgments

The authors acknowledge financial support by ERC Project "Adequate", ANR-11-IDEX-0005-02 (Labex SEAM Project "Capture") and the network "Salles Blanches Paris Centre".